Transient model for electrical activation of aluminium and phosphorus-implanted silicon carbide

V. Šimonka, A. Toifl, A. Hössinger, S. Selberherr, and J. Weinbub

Citation: Journal of Applied Physics **123**, 235701 (2018); doi: 10.1063/1.5031185
View online: https://doi.org/10.1063/1.5031185
View Table of Contents: http://aip.scitation.org/toc/jap/123/23
Published by the American Institute of Physics

Transient model for electrical activation of aluminium and phosphorus-implanted silicon carbide

V. Šimonka,[1,a)] A. Toifl,[2] A. Hössinger,[3] S. Selberherr,[2] and J. Weinbub[1]
[1]*Christian Doppler Laboratory for High Performance TCAD, Institute for Microelectronics, TU Wien, Gußhausstraße 27-29/E360, 1040 Wien, Austria*
[2]*Institute for Microelectronics, TU Wien, Gußhausstraße 27-29/E360, 1040 Wien, Austria*
[3]*Silvaco Europe Ltd., Compass Point, St Ives, Cambridge PE27 5JL, United Kingdom*

(Received 29 March 2018; accepted 30 May 2018; published online 19 June 2018)

The development of novel electron devices requires a continuous support by process and device simulations in order to improve electrical properties and reduce production costs. However, an accurate description of the electrical properties of impurities in silicon carbide – a key wide bandgap semiconductor for power devices – is currently not available, which significantly limits the predictability of critical fabrication processes. Here, we introduce a transient model for electrical activation of implanted aluminium and phosphorus in silicon carbide to fill this gap. Our results suggest differences between acceptor- and donor-type dopants including activation speed, saturation limit, and activation regions. We predict acceptor and donor concentrations according to the various annealing times, temperatures, and doping concentrations. The results are used for the fabrication of PN-junction diodes, which are characterized and compared with the experimental findings. Finally, we predict improvements of various annealing steps, i.e., increased active concentration, increased carrier concentration, and decreased sheet resistance, and perform a comprehensive comparison with experimental data to evaluate the proposed model. *Published by AIP Publishing.*
https://doi.org/10.1063/1.5031185

I. INTRODUCTION

The dominant semiconductor for power devices has for a long time been silicon (Si). However, Si-based devices have already reached their physical limit regarding capabilities for high-voltage, high-frequency, and high-temperature applications. Wide bandgap (WBG) semiconductors, in particular, silicon carbide (SiC) and gallium nitride (GaN), are attractive replacements for traditional Si in order to increase the device performance properties and reduce internal device losses.[1] The advantageous properties, which enable significant improvements of power devices, include higher thermal conductivity, higher breakdown field, and higher carrier saturation velocity, compared to Si. Among the WBG semiconductors, SiC has the highest thermal conductivity and is thus the most desirable material for high-power applications. SiC exists in various crystalline forms, such as 3C, 4H, 6H, and 15R, and can be selectively doped with donor- or acceptor-type impurities. It has been shown that 4H-SiC exhibits the best physical properties for power device fabrication[1] and is thus in the focus of this study. The physical properties of Si, GaN, GaAs, 4H-SiC, and 6H-SiC are summarized in Fig. 1 for comparison. However, fabrication steps of SiC devices have not yet been fully optimized,[2–4] even though the need to decrease production costs of semiconductor devices is tremendous.[5]

The most used technology for selective doping is currently ion implantation,[6] particularly due to the low costs relative to the other alternative doping techniques. Typically, implantation requires a post-implantation annealing treatment in order to repair crystal damage from the ion bombardment and to facilitate electrical activation of dopants. However, the mechanism of dopant activation in SiC is not fully understood.[7] In particular, a modeling approach to describe the transient activation process is completely missing.[8] The difficulties are associated with the high annealing temperatures and the deep ionization energies of implanted species. This lack of ability to predict the activation concentration after particular annealing steps significantly limits the predictability of process technology computer-aided design (TCAD) and, therefore, impedes overall device fabrication optimization.

In this paper, a comprehensive study of the dopant-specific annealing step is presented with respect to the total doping concentration and annealing temperature. We introduce a time-dependent, i.e., transient, model with empirical evaluations according to experimental data in Sec. II. The obtained parameters have been implemented into the Silvaco's Victory Process simulator[9] and a series of full process and device simulations of SiC-based PN-junction diodes have been performed and compared with the experimental findings in Sec. III.

II. METHOD

The preferred acceptor-type dopant species in SiC is aluminium (Al) for low resistivity applications,[10] while the preferred donor-type dopant is phosphorus (P), when high-dose implantation is required.[11] In addition, implantation and annealing steps of Al and P show potential for a wide utilization of SiC devices,[11–14] which is the reason, why we focus on Al and P-implantation of 4H-SiC. We have created a comprehensive collection of experimental data of various

a)Electronic mail: simonka@iue.tuwien.ac.at

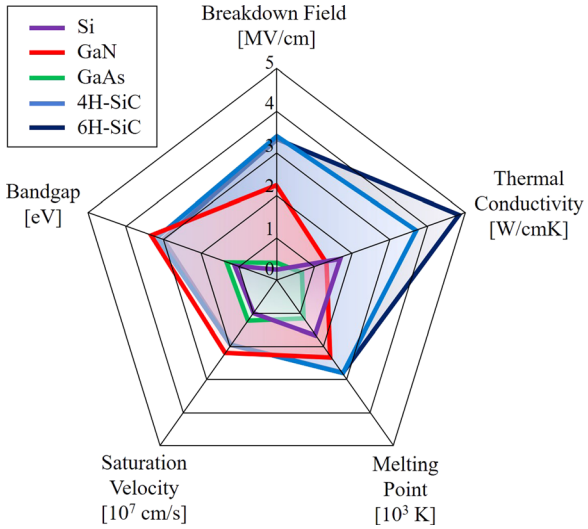

FIG. 1. Comparison of the physical properties of Si, GaN, GaAs, 4H-SiC, and 6H-SiC.

post-implantation steps of Al and P impurities in SiC. The acceptor[12,14–19] and donor[1,11,18,20–22] concentrations have been obtained from previous experimental studies for various annealing temperatures, annealing times, and total implanted concentrations. The collection of the Al and P-implanted data is plotted as a function of annealing time in Fig. 2. The experimental data has been selected such that identical crystal orientations, annealing ambient, implantation temperatures, and measuring methods are considered. This is particularly important for this study as it enables proper model fitting for predicting annealing temperature, annealing time, and total concentration.[23] We have assumed that the different annealing methods (microwave, inductive, and resistive heating) result in equal activation ratios.[8] All of the selected data is based on annealing in argon (Ar) ambient. In addition, no differences in activation rates between 4H and 6H-SiC are assumed.[19] According to the available experimental data, the error due to this assumption is less than 5%.

The model for electrical activation of dopants in SiC has been inherited and modified from the model for Si,[9] which is described with a differential equation and represents the reaction of the dopants' activation processes. The active concentration of dopants in SiC is

$$\frac{dC_{act}}{dt} = -\kappa\left(C_{act} - \frac{C_{tot}}{1+\frac{C_{tot}}{C_{ss}}}\right). \quad (1)$$

C_{tot} is the total implanted concentration of dopants. C_{ss} and κ are the solid solubility and characteristic reaction rate, respectively, and are the key parameters of the model, obtained by model fitting. In the case of SiC, C_{act} is approximated to be equal to the electrically measured (i.e., Hall and sheet resistance measurements) acceptor (N_A) or donor concentration (N_D), which originate from the ionized dopants only. C_{ss} is the limiting parameter for the total active concentration and κ is the limiting parameter for the reaction rate of the activation mechanism, i.e., the slope of the curve.

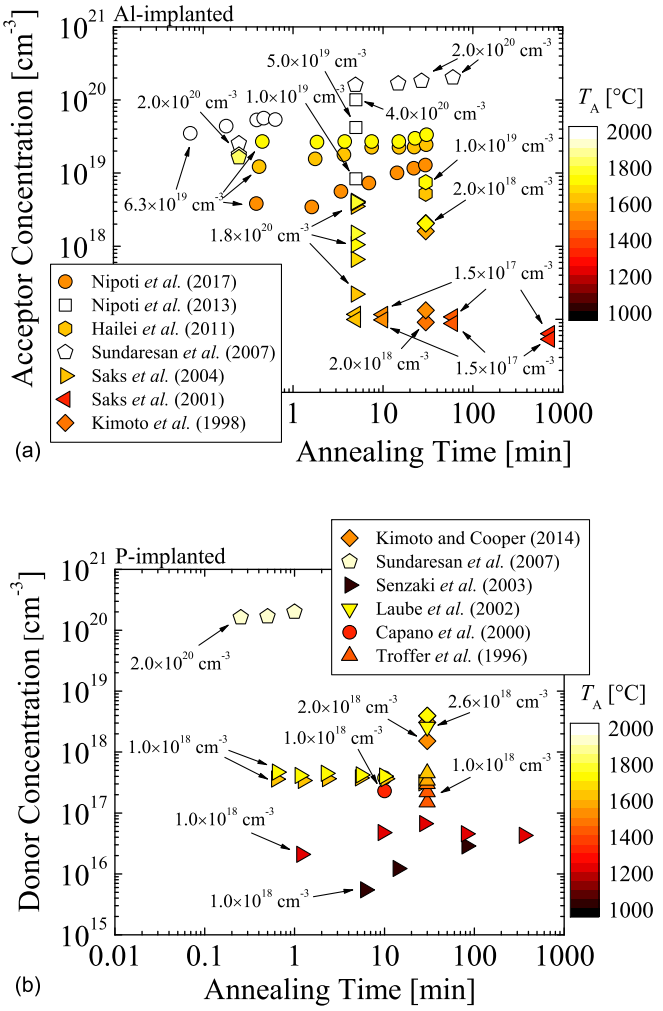

FIG. 2. (**a**) Acceptor and (**b**) donor concentrations as a function of annealing time for various total concentrations and annealing temperatures. The data has been taken from previous experimental studies for acceptor[12,14–19] and donor[1,11,18,20–22] type doping. The text and arrows within the figures refer to the total implanted concentration of the corresponding data sets.

Several iterations of the least squares approximation[24] have been performed for each individual data set to ensure a minimal numerical error, when fitting the proposed activation model (1) to the data shown in Fig. 2. The fitting parameters are C_{ss} and κ, which are obtained for each annealing temperature individually. The temperature-dependent parameters are then additionally fitted with the Arrhenius equation[25] to ensure a continuous, interpolated, and extrapolated dependence on the annealing temperature. The calibrated Arrhenius parameters, i.e., activation energy E_a and pre-exponential factor Z, are summarized in Table I. C_{ss} and κ for Al and P-implanted SiC as well as the corresponding

TABLE I. Arrhenius parameters, i.e., activation energy and pre-exponential factor, of the solid solubility and characteristic rate for Al and P-implanted SiC.

	C_{ss}		κ	
Dopant	Z (cm^{-3})	E_a (eV)	Z (1/min)	E_a (eV)
Al	1.21×10^{26}	2.58	5.83×10^{6}	2.72
P	7.17×10^{23}	2.09	6.51×10^{3}	1.38

Arrhenius plots are shown in Fig. 3. The activation energy for Al-implanted SiC is for both parameters (C_{ss} and κ) higher, compared to P-implanted SiC. C_{ss} is for relatively low temperatures (around 1150 °C) identical for Al and P impurities. On the contrary, κ is for Al and P identical for relatively high temperatures around 1950 °C. For the steady-state solution of the model, i.e., the solution for the thermal equilibrium, C_{ss} plays a significant role by defining the upper limits of the active concentration of the dopants for particular annealing temperatures. Moreover, C_{ss} varies for up to an order of magnitude between the Al and P dopants for high temperatures. Additionally, the Arrhenius plots suggest that the solubility limit for Al-implanted SiC is higher, compared to P-implanted SiC.

III. RESULTS AND DISCUSSION

The proposed transient activation model together with the obtained model parameters enable the prediction of the transient active concentration or activation ratio after thermal annealing steps of SiC device fabrication. In this section, the calibrated model is analyzed and the model results are validated based on the gathered experimental data. In particular, in-depth modeling and parameter aspects are discussed, followed by actual process simulations of representative PN-junction diodes including validations with experimental data. These analyses are concluded with evaluating the electrical characteristics via device simulations in comparison to experimental data.

A. Modeling

We have calculated the speed of the activation process of Al and P-implanted SiC, as shown in Fig. 4. The results are calculated for the common industry-related[1] implanted concentration of $1 \times 10^{18}\,\mathrm{cm}^{-3}$ and various annealing temperatures, i.e., 1400, 1600, 1800, 2000, and 2200 °C. The results show that for high T_A, the initial activation speed is extremely high and decreases rapidly with time. This implies that the activation process for high T_A is mostly significant for $t_A < 5$ min. In contrast, for low T_A, the initial activation speed is a few orders of magnitude lower and decreases slowly, thus $t_A > 15$ min is required for the effective activation of impurities. As shown in the inset figures, the activation process for T_A = 1800, 2000, and 2200 °C is almost instant and achieves 100% activation. This indicates that rapid thermal annealing methods are indeed suitable for the activation of dopants in SiC, provided that the annealing temperatures are above ≈1700 °C. In order to investigate the differences between the acceptor and donor type impurities in detail, we have conducted a parameter analysis.

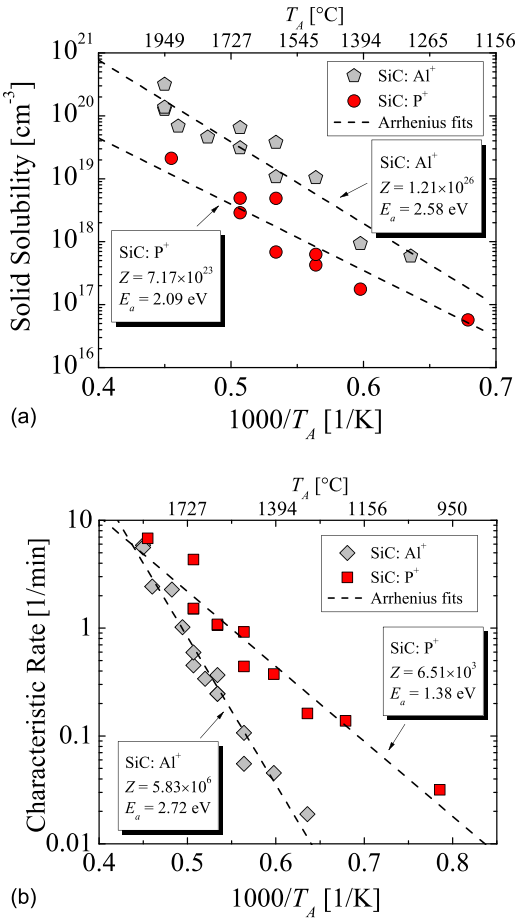

FIG. 3. Model parameter **(a)** solid solubility and **(b)** characteristic rate for Al (closed) and P-implanted (open symbols) SiC. The dashed lines refer to the fits with the Arrhenius equation.

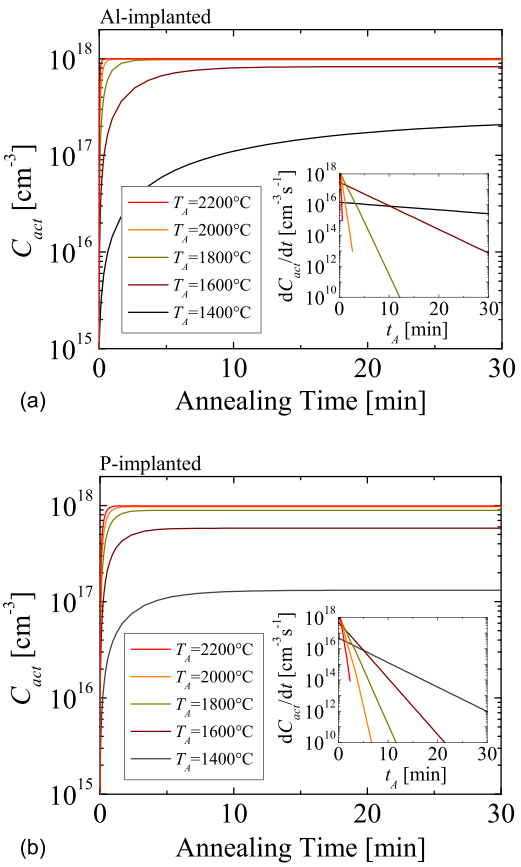

FIG. 4. Active concentration as a function of annealing time for **(a)** Al and **(b)** P-implanted SiC. Calculations are performed for $C_{tot} = 10^{18}\,\mathrm{cm}^{-3}$ and various annealing temperatures. The inset figures show the speed of the activation mechanism (dC_{act}/dt) as a function of annealing time for the respective annealing temperatures.

We have performed a parameter study based on numerous (i.e., 10^6) calculations of Al and P implantations in SiC, followed by various annealing steps. Phase diagrams of activation regions as a function of annealing temperature and annealing time are shown in Fig. 5. Due to the Arrhenius fitting of the parameters, the results are extrapolated for certain annealing temperatures, shown with the dashed lines. The phase diagrams enable an estimation of the minimally required T_A and t_A to acquire full (i.e., above 90%) activation of the implanted SiC region. The phase diagrams additionally show that the phase region $0.1 < R_{act} < 1.0$ is smaller for Al acceptors than for P donors. The difference in those areas indicates that P acceptors require less energy for activation than P donors, which is consistent with experimental findings.[1] This figure in addition shows the approximation of the steady-states for an arbitrary annealing temperature. For instance, at 1700 °C the steady-state for Al acceptors is reached for an annealing time above ≈25 min and for P donors above ≈3 min, i.e., the activation ratio is not affected beyond these times.

One of the significant issues of WBG semiconductors is that the rate of the dopant activation after high dose implantation (i.e., above $10^{18}\,cm^{-3}$) significantly decreases,[12] i.e., saturates.[8] In order to investigate the saturation effects due to high implantation doses, we have performed a parameter study, producing phase diagrams of activation regions as a function of annealing temperature and total implanted concentration, as shown in Fig. 6. These results suggest that the saturation region of the activation mechanism in SiC is temperature-dependent. As the annealing temperature increases, the boundary of the saturation region, shown with the dashed red lines, increases as well. This indicates that for annealing steps with high T_A, the doping doses can be a few orders of magnitude higher than with a low T_A, while maintaining the same ratio of activation. The model predicts that annealing steps with T_A below 1000 °C for Al-implanted and 850 °C for P-implanted SiC, do not contribute to the improvement of electrical properties, regardless of the doping dose. The white region of the phase diagram, which refers to the full dopant activation, is larger for the Al-implanted SiC compared to P-implanted SiC. This indicates that a wider span of the parameter variety can be chosen for the acceptor-type doping, while maintaining the desired high activation ratio > 90%. These findings support the latest trend of Al being the preferable dopant for SiC implantation technology.[5,10,26]

B. Simulations

The model and the parameters from this study have been implemented into the Silvaco's Victory Process simulator.[9] Various PN-junction diodes have been processed and evaluated according to our model predictions. Each of the

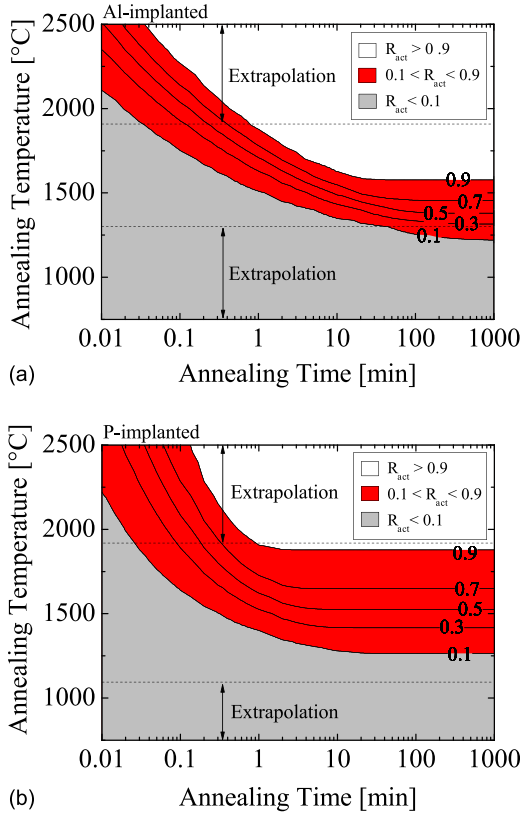

FIG. 5. Phase diagrams of electrical activation as a function of annealing temperature and annealing time for **(a)** Al and **(b)** P-implanted SiC. Simulations are performed for the total concentration $C_{tot} = 10^{18}\,cm^{-3}$. The gray, red, and white regions refer to the low, intermediate, and high activation of SiC impurities, respectively. The dashed lines are the extrapolation boundaries.

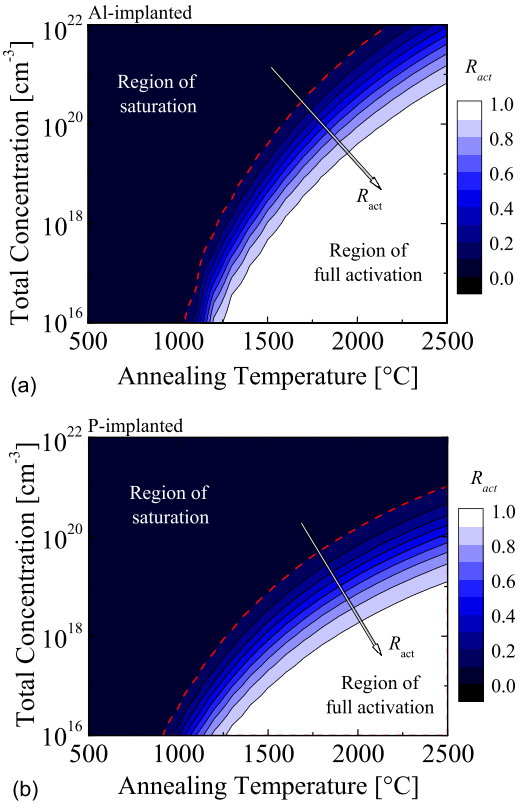

FIG. 6. Phase diagrams of electrical activation as a function of annealing temperature and total concentration for **(a)** Al and **(b)** P-implanted SiC. The simulations were performed for an annealing time $t_A = 1000$ min, i.e., steady-state. The colors indicate various activation ratios (R_{act}) and the red dashed lines indicate the boundaries of the saturation regions.

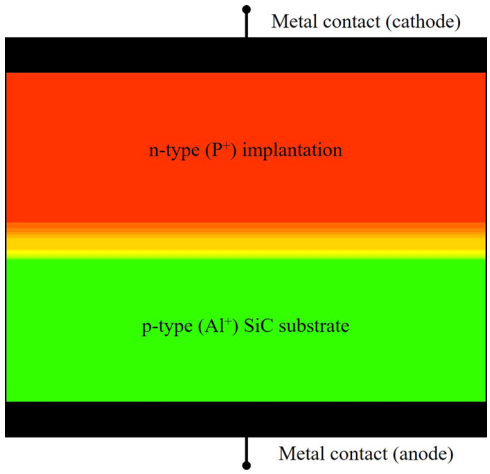

FIG. 7. Schematic design of the PN-junction diode used in simulations. The red and green regions refer to the n- and p-type regions, respectively. The black regions indicate the ohmic contacts, i.e., the cathode and anode.

simulated PN-diodes varies in the annealing temperature, annealing time, and/or total concentration. An exemplary device structure is shown in Fig. 7 and the respective doping parameters are given in Table II. The device processing setups are based on three different experimental investigations,[11,13,22] which have been chosen to ensure a focused study of the annealing process. All of the setups include implantation of P in an Al-doped SiC substrate. The investigated SiC orientation is (0001) Si-face. The simulated processing steps are: (1) p-type (Al-doped) SiC substrate. (2) n-type (P) implantation according to the chosen setup. The Monte Carlo implantation model from the Victory Process simulator has been utilized. (3) Deposition of silicon dioxide (SiO_2). (4) Annealing of implanted species according to the results from experimental setups. This step includes the proposed model and parameters. (5) Removal of SiO_2. (6) Deposition of metal for contacts on the top and bottom of the device.

The depth profiles, i.e., P concentration and donor concentration, of the two implantation setups and simulations are shown in Fig. 8. The solid lines refer to the results from the process simulations and the symbols refer to the experimental findings. The red color indicates the implanted profiles of both simulations and experiments. The simulated implanted profiles of Setup 1 [Fig. 8(a)] and 2 [Fig. 8(b)] are identical to the profiles from the corresponding references. The implanted species are annealed for 30 min at 1700 °C and 30 min at 1550 °C in the case of Setup 1 and for 30 min

TABLE II. Implantation setups for the p-type SiC (0001) Si-face.

Setup	1	2	3
Reference	Schmid *et al.*[13]	Troffer *et al.*[22]	Senzaki *et al.*[11]
Substrate Al^+ Concentration (cm^{-3})	1.0×10^{16}	1.3×10^{17}	5.0×10^{15}
Implanted P^+ Energies (keV)	70, 180, 320, 500, 750	70, 160, 280, 450, 600, 800, 1100, 1500, 2000	40, 70, 160, 180, 220, 250
Total fluence (cm^{-2})	1.4×10^{16}	1.3×10^{14}	7.0×10^{15}

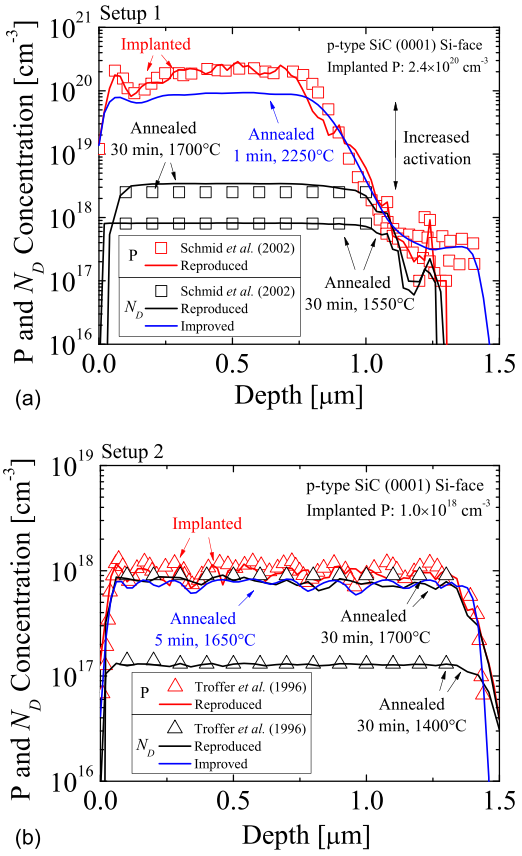

FIG. 8. Depth profiles of P concentration and donor concentration utilizing implantation (**a**) Setup 1 and (**b**) Setup 2. The red and black symbols are P and N_D from Refs. 13 and 22, respectively, the red and black lines are the reproduced P and N_D, respectively, and the blue lines are the predicted N_D.

at 1700 °C and 30 min at 1400 °C in the case of Setup 2. The deviation between the results from simulation and experiment for the annealed samples is very small, in average $\sigma < 3\%$. This indicates that the proposed model captures the key characteristics of the activation mechanism and provides an accurate prediction of the activation levels. It can be seen from Fig. 8(a) that a very low activation ratio of high-dose acceptor-type impurities is achieved after the typical annealing step, i.e., 30 min at 1700 °C. Furthermore, we provide an estimate of the required processing variables for sufficient (>90%) activation. Experimental methods have not been able to provide such an estimate due to technical reasons.[13] The prediction, based on the proposed model (blue lines), is that the activation of high-dose implantation is significantly improved after the annealing step of 1 min at 2250 °C. In this case of high-dose implantation, N_D has been increased from $3 \times 10^{18}\,cm^{-3}$ to $6 \times 10^{19}\,cm^{-3}$. Moreover, such simulations can provide an estimate for the shortest annealing time and lowest annealing temperature, which result in a desired active concentration. For instance, for Setup 2, we show that an annealing step of 5 min at 1650 °C is sufficient to achieve an identical activation when annealing for 30 min at 1700 °C. This modification introduces a very small variation in the dopant activation, i.e., the activation ratio is preserved, but on the other hand, the potential for reduction of production costs due to shorter high-temperature annealing is provided.

According to the obtained depth profiles of Setup 1 and Setup 2, we have performed device simulations to characterize the electrical properties of the implanted SiC after the investigated annealing steps. In order to characterize the processed PN-diodes, we have investigated a fundamental quantity, i.e., the carrier concentration as a function of sample temperature, shown in Fig. 9. Comparing the experimental data (red symbols) and simulation results (black lines) clearly demonstrates a very low deviation, in average $\sigma < 1\%$. The PN-junction diode, processed with the previously proposed annealing step from Setup 1, shows improved device characteristics (Fig. 9(a), blue line). The carrier concentration is significantly increased, i.e., by an order of magnitude, which provides better overall device operation. Moreover, the diode, which is fabricated with the proposed annealing step from Setup 2 (i.e., reduced time and temperature), shows almost identical behaviour (Fig. 9(b), blue line) as the diode with the non-modified annealing step. Small variations between the two annealing steps are seen in extreme operation temperatures, i.e., below 150 K and above 700 K, but are almost identical in the typical device operation regime, i.e., 200–600 K. Thus, the shorter annealing step is perfectly sufficient and at the same time provides a cost reduction.

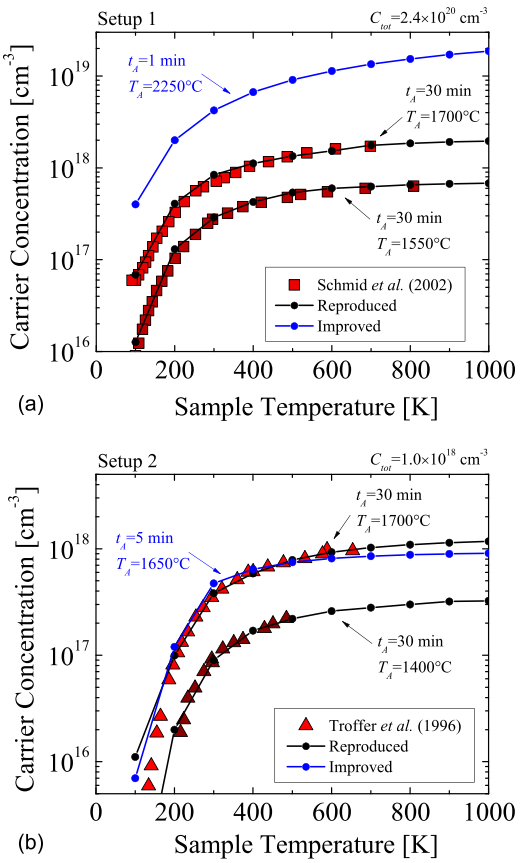

FIG. 9. Carrier concentration as a function of sample temperature utilizing implantation **(a)** Setup 1 and **(b)** Setup 2. The symbols refer to Refs. 13 and 22, the black lines are the simulation results from reproduced depth profiles, and the blue lines are simulation results from predicted depth profiles. The reproduced and predicted depth profiles are shown in Fig. 8.

We have further verified the simulation capabilities of our model by processing SiC diodes based on the implantation and annealing parameters of Setup 3 (cf. Table II). Numerous process simulations of the PN-junction diodes have been performed followed by device simulations to obtain the current-voltage (IV) characteristics of each individual device. This approach, i.e., numerous process simulations, which are distinctive in the annealing variables only, provides a focused investigation of the annealing steps. Various t_A from 0.01 min to 1000 min at T_A from 1200 °C to 1700 °C have been investigated. The IV plots for various t_A and T_A are shown in Fig. 10. For the sake of readability, we show only the two extreme conditions, i.e., $T_A = 1200$ and 1700 °C. The knee voltage is, regardless of the processing conditions, ≈2.5 V, which is approximately three-times higher than that of an equivalent diode based on Si. It is clear from the results, that both annealing variables, T_A and t_A, significantly affect the slope of the IV diagrams.

The IV plots (Fig. 10) have been used to calculate the resistance-time (Rt) characteristics of each individual device. The sheet resistance is obtained from the slope of the IV plots and the diode geometries for various t_A and T_A, as shown in Fig. 11. For $T_A > 1600$ °C the sheet resistance decreases until $t_A \approx 1$ min, which implies once more that for high annealing temperatures a rapid annealing step is sufficient. In this case, no significant decrease in the sheet resistance is observed for $t_A > 1$ min. On the other hand, the low-temperature annealing step shows a continuous decrease in the sheet resistance over 1000 min. The figure in addition suggests that the sheet resistance is reduced for more than 500 Ω/□ between the annealing step of $T_A = 1200$ and 1700 °C. The comparison of our results (solid lines) to the experimental findings (symbols) shows a very good agreement, i.e., in average less than 5% deviation. This implies that the proposed model provides a very accurate prediction of the annealing temperature-dependent sheet resistance of SiC devices.

IV. CONCLUSIONS

A transient model to predict activation of impurities in SiC has been proposed, calibrated, and verified to accurately

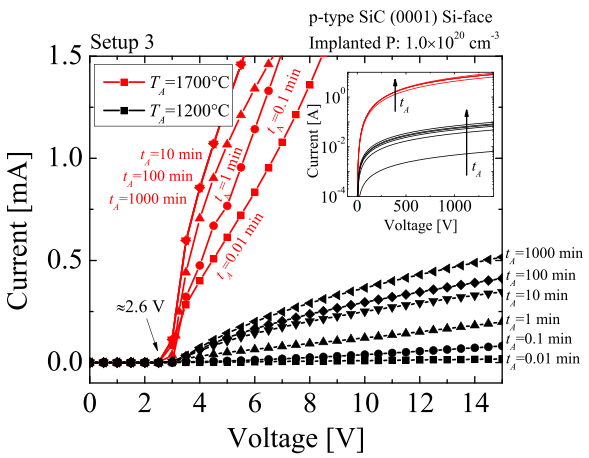

FIG. 10. Current as a function of voltage of the PN-junction diodes annealed for $t_A = 0.01$, 0.1, 1, 10, 100, and 1000 min at $T_A = 1200$ and 1700 °C, utilizing implantation Setup 3.

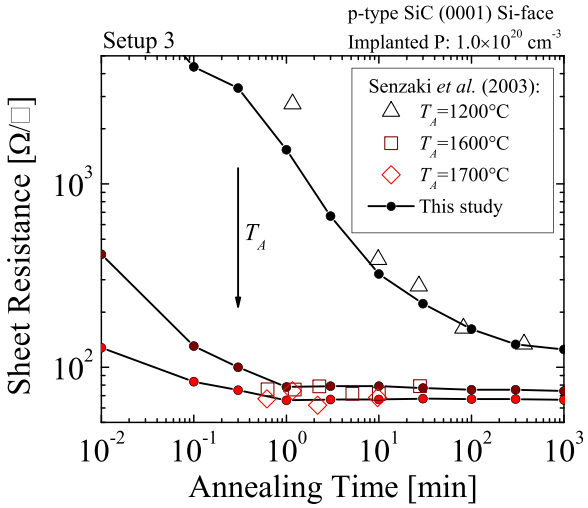

FIG. 11. Sheet resistance as a function of annealing time of the PN-junction diodes annealed for various t_A at T_A = 1200, 1600, and 1700 °C, utilizing implantation Setup 3. The symbols refer to the experimental data[11] and the lines are results from our simulations.

reproduce devices features during operation in various conditions. The parameters obtained in this study have been implemented in the Silvaco's Victory Process simulator and numerous process and device simulations of PN-junction diodes have been performed to characterize the properties of the model. The electrical activation ratios of Al and P-implanted SiC have been reproduced and the accountable time evolution of the activation process has been predicted. The results show that the minimal T_A for full activation of Al and P dopants with C_{tot}=10^{18} cm^{-3} is 1600 °C and 1800 °C, respectively. For cases of $t_A < 1$ min, the dopants are fully activated for $T_A > 2000$ °C. In addition, our results suggest that the saturation effects of the activation process are temperature-dependent. Furthermore, comprehensive comparisons with experimental data have been performed to evaluate the findings of this study. Our results show in average $< 5\%$ deviation. Finally, we have suggested improvements for the electrical characteristics, i.e., increased donor concentration, decreased resistance, and reduced t_A and T_A, to optimize the fabrication steps of SiC devices according to the model predictions.

ACKNOWLEDGMENTS

The financial support by the Austrian Federal Ministry for Digital and Economic Affairs and the National Foundation for Research, Technology and Development is gratefully acknowledged.

[1]T. Kimoto and J. A. Cooper, *Fundamentals of Silicon Carbide Technology: Growth, Characterization, Devices and Applications* (John Wiley and Sons, 2014).
[2]M. I. Idris, M. H. Weng, H. Chan, A. Murphy, D. A. Smith, R. Young, E. P. Ramsay, D. T. Clark, N. G. Wright, and A. B. Horsfall, "Electrical stability impact of gate oxide in channel implanted SiC NMOS and PMOS transistors," Mater. Sci. Forum **897**, 513–516 (2017).
[3]R. Radhakrishnan, M. F. MacMillan, and R. L. Woodin, "Doping engineering to enhance performance of a silicon carbide power device," in *Proceedings of the Workshop on Wide Bandgap Power Devices and Applications (WiPDA)* (2016), pp. 105–107.
[4]V. Šimonka, A. Hössinger, J. Weinbub, and S. Selberherr, "Growth rates of dry thermal oxidation of 4H-silicon carbide," J. Appl. Phys. **120**, 135705 (2016).
[5]R. Nipoti, A. Parisini, G. Sozzi, M. Puzzanghera, A. Parisini, and A. Carnera, "Structural and functional characterizations of Al$^+$ implanted 4H-SiC layers and Al$^+$ implanted 4H-SiC pn junctions after 1950 C post implantation annealing," ECS J. Solid State Sci. Technol. **5**, P621–P626 (2016).
[6]J. Weisse, M. Hauck, T. Sledziewski, M. Tschiesche, M. Krieger, A. Bauer, H. Mitlehner, L. Frey, and T. Erlbacher, "Analysis of compensation effects in aluminum-implanted 4H–SiC devices," Mater. Sci. Forum **924**, 184–187 (2018).
[7]V. Šimonka, A. Hössinger, J. Weinbub, and S. Selberherr, "Modeling and simulation of electrical activation of acceptor-type dopants in silicon carbide," Mater. Sci. Forum **924**, 192–195 (2018).
[8]V. Šimonka, A. Hössinger, J. Weinbub, and S. Selberherr, "Empirical model for electrical activation of aluminium and boron doped silicon carbide," IEEE Trans. Electron Devices **65**, 674–679 (2018).
[9]See https://www.silvaco.com/products/tcad/ (18.04.2017) for Silvaco's Victory Process simulator.
[10]A. Parisini and R. Nipoti, "Analysis of the hole transport through valence band states in heavy Al doped 4H-SiC by ion implantation," J. Appl. Phys. **114**, 243703 (2013).
[11]J. Senzaki, K. Fukuda, and K. Arai, "Influences of postimplantation annealing conditions on resistance lowering in high-phosphorus-implanted 4H-SiC," J. Appl. Phys. **94**, 2942–2947 (2003).
[12]N. Saks, A. Suvorov, and D. Capell, "High temperature high-dose implantation of aluminum in 4H-SiC," Appl. Phys. Lett. **84**, 5195–5197 (2004).
[13]F. Schmid, M. Laube, G. Pensl, G. Wagner, and M. Maier, "Electrical activation of implanted phosphorus ions in [0001] and [11-20]-oriented 4H-SiC," J. Appl. Phys. **91**, 9182–9186 (2002).
[14]T. Kimoto, O. Takemura, H. Matsunami, T. Nakata, and M. Inoue, "Al$^+$ and B$^+$ implantations into 6H-SiC epilayers and application to PN junction diodes," J. Electron. Mater. **27**, 358–364 (1998).
[15]R. Nipoti, A. Carnera, G. Alfieri, and L. Kranz, "About the electrical activation of 1 × 10^{20} cm^{-3} ion implanted Al in 4H–SiC at annealing temperatures in the range 1500–1950 °C," Mater. Sci. Forum **924**, 333–338 (2018).
[16]R. Nipoti, R. Scaburri, A. Hallén, and A. Parisini, "Conventional thermal annealing for a more efficient p-type doping of Al$^+$ implanted 4H-SiC," J. Mater. Res. **28**, 17–22 (2013).
[17]W. Hailei, S. Guosheng, Y. Ting, Y. Guoguo, W. Lei, Z. Wanshun, L. Xingfang, Z. Yiping, and W. Jialiang, "Effect of annealing process on the surface roughness in multiple Al implanted 4H-SiC," J. Semicond. **32**, 072002 (2011).
[18]S. G. Sundaresan, M. V. Rao, Y.-L. Tian, M. C. Ridgway, J. A. Schreifels, and J. J. Kopanski, "Ultrahigh-temperature microwave annealing of Al$^+$- and P$^+$- implanted 4H-SiC," J. Appl. Phys. **101**, 073708 (2007).
[19]N. Saks, A. Agarwal, S. Ryu, and J. Palmour, "Low-dose aluminum and boron implants in 4H and 6H silicon carbide," J. Appl. Phys. **90**, 2796–2805 (2001).
[20]M. Laube, F. Schmid, G. Pensl, G. Wagner, M. Linnarsson, and M. Maier, "Electrical activation of high concentrations of N$^+$ and P$^+$ ions implanted into 4H-SiC," J. Appl. Phys. **92**, 549–554 (2002).
[21]M. A. Capano, J. Cooper, Jr., M. Melloch, A. Saxler, and W. Mitchel, "Ionization energies and electron mobilities in phosphorus and nitrogen-implanted 4H-silicon carbide," J. Appl. Phys. **87**, 8773–8777 (2000).
[22]T. Troffer, C. Peppermüller, G. Pensl, K. Rottner, and A. Schöner, "Phosphorus-related donors in 6H-SiC generated by ion implantation," J. Appl. Phys. **80**, 3739–3743 (1996).
[23]V. Šimonka, A. Hössinger, J. Weinbub, and S. Selberherr, "Modeling of electrical activation ratios of phosphorus and nitrogen doped silicon carbide," in *Proceedings of the International Conference on Simulation of Semiconductor Processes and Devices (SISPAD)* (2017), pp. 125–128.
[24]B. Wendroff, *Theoretical Numerical Analysis* (Elsevier, 2014).
[25]S. Arrhenius, *Über die Dissociationswärme und den Einfluss der Temperatur auf den Dissociationsgrad der Elektrolyte* (Wilhelm Engelmann, 1889).
[26]T. Kimoto, K. Kawahara, N. Kaji, H. Fujihara, and J. Suda, "Ion implantation technology in SiC for high-voltage/high-temperature devices," in *Proceedings of the International Workshop on Junction Technology (IWJT)* (2016), pp. 54–58.